Defect and Diffusion Forum Vols. 283-286 (2009) pp 425-431
online at http://www.scientific.net

Online available since 2009/Mar/02

Fundamental Studies on the Transient Stages of Scale Growth in Fe-22 wt.% Cr Alloys

L. M. Fernandez Diaz[1,2,a], J. Zhu[1,2,b], G.R. Holcomb[3,c], P.D. Jablonski[3,d], D.E. Alman[3,e], S. Sridhar[1,2,f]

[1]National Energy Technology Laboratory, Pittsburgh, PA 15236, USA

[2]Department of Materials Sciences and Engineering, Carnegie Mellon University, Pittsburgh, PA 15213, USA

[3]National Energy Technology Laboratory, Albany, OR 97321-2198, USA

[a]lauramfd@andrew.cmu.edu, [b]jingxiz@andrew.cmu.edu, [c]Gordon.Holcomb@netl.doe.gov, [d]Paul.Jablonski@netl.doe.gov, [e]David.Alman@netl.doe.gov, [f]sridhars@andrew.cmu.edu

Keywords: Reactive elements, Cr_2O_3 scale growing, high temperature oxidation, Fe based alloys.

Abstract. It is known that additions of reactive elements such as Ce, La or Y improve the properties of protective oxide-scales on Ni and Fe based alloys [1-3] by increasing oxide adhesion, decreasing the transient time until a continuous Cr_2O_3 layer is formed and decreasing the parabolic rate constant. Nevertheless, the precise roles played by these reactive elements to improve scales and the precise mechanisms by which they are incorporated into the scale during the surface treatment processes are unknown. Although they are believed to be associated with transport properties in the scale, it is not clear how this occurs or why it improves oxidation resistance. This project is aimed to gain understanding of the scale evolution in Fe-22 wt.% Cr alloys at 800 ^oC in dry air during the transient stage after 15 minutes of oxidation. The effect of La (120 and 290 ppm) and Ce (270 and 610 ppm) additions added during melt-stage processing are investigated. The surface oxidation process was imaged in-situ through a Confocal Scanning Laser Microscope (CSLM) and the results were correlated with post-experiment characterization through FEG-SEM and FIB-SEM combined with 3D reconstruction. The roles of rare-earth oxide particles on nucleation of Cr_2O_3 and blockage of short-circuit diffusion paths in the oxide scale and underlying metal are discussed.

Introduction

The influence of reactive elements (RE) on lowering alloy-oxidation rates has well established [1-4] but quantitative details on this effect are lacking and several mechanisms have been suggested.
Ecer and Meier studied the oxidation mechanism of Ni-Cr alloys containing 44 and 50 wt. % Cr [5]. The oxidation process was found to be complex and it could not be described by a single model. The growth of the Cr_2O_3 oxide occurs by outwards Cr diffusion. Cr vapor is transported to the scale, resulting in scale bulging and cracking and voids incorporation. Giggins and Pettit studied the effect of ThO_2 dispersion in Ni-Cr alloys [4]. As a result of Cr oxidation ThO_2 particles get enriched in the alloy near the interface, preventing supply of Cr atoms in the alloy to the scale. Concerns about this proposed model are the shortage of ThO_2 particles to block the Cr diffusion [4]. Stringer et al. [1] proposed that dispersed CeO_2 and Y_2O_3 in Ni-Cr alloys act as nucleation sites for Cr_2O_3. Ecer and Meier showed the effects of Ce additions on Ni-Cr alloys [2] and the superficial application of CeO_2 powders on Ni-Cr and Fe-Cr alloys [3]. RE oxides are suggested to act as nucleation sites while cerium ions would segregate to the oxide grain boundaries and decreasing the transport though them. Migration of the solute cloud with the grain boundary has also been proposed, involving a reduced level of atomic movement at the boundary. Thanneeru et al. [6] studied the high-temperature oxidation kinetics of 304 steels in the presence of nanocrystalline ceria (NC) and La^{3+}

doped nanocrystalline ceria (LDN) coatings. Slower scale growth and finer grain structure with increased porosity as the La concentration was augmented in LDN coatings were found.
In this paper we focus on the state of oxidation after 15 minutes of oxidation in air at 800°C, which would fall within the transient stage of the scale development [7]. The objective is to characterize the scales for three Fe-22 wt.%Cr alloys containing zero RE, 120 ppm La + 270 ppm Ce and 290 ppm La + 610 ppm Ce, respectively.

Experimental

Alloys with different mischmetal levels were prepared based on a nominal composition of Fe-22Cr-0.5Mn-0.1Ti (weight percent alloys). Glow Discharge Mass Spectroscopy (GDMS) was used to analyze rare earth element content of the alloys, as summarized in Table 1 below.

Sample chemistries.

El./Mat	F_1	F_2	F_3	El/Mat	F_1	F_2	F_3
	[wt%]	[ppm wt]			[wt%]	[ppm wt]	
B		0.03	0.02	**Mn**	0.43	0.55 [wt%]	0.56 [wt%]
F		<0.01	<0.01	**Fe**	76.96	Matrix	Matrix
Na		0.03	0.04	**Co**	<0.010	23	23
Mg		0.12	0.20	**Cu**	0.0064	8.4	8.4
Al	0.16	320	330	**Zn**		<5	<5
Si	0.021	16	8.3	**Y**		<0.5	<0.5
P	<0.001	16	16	**Zr**		0.82	0.91
S		32	46	**Nb**		=<30	=<30
Cl		0.04	0.12	**Mo**	<0.010	4.1	1.7
K		<0.05	<0.05	**La**		120	290
Ca		0.14	0.12	**Ce**		270	610
Ti	0.1	720	770	**Pr**		23	54
V	<0.010	10	12	**Nd**		8.2	19
Cr	22.18	Matrix	Matrix	**C**	0.002	0.005 [wt%]	0.019 [wt%]
Ni	0.11			**Ta**	0.0039		
W	0.017			**Nb**	0.003		

Table 1. Composition of F_1, F_2 and F_3.

Samples were polished using SiC paper number 320 and subsequently numbers 800 and 1200. Grinding was done using diamond paste suspensions of 6, 3 and 1 μm. For metallographic investigation, samples were mounted and then etched using mixed acids: 15 parts hydrochloric acid, 10 parts nitric acid, 10 parts acetic acid and few drops of glycerin as a wetting agent were added for each small quantity (~50 ml) of etchant. Images were obtained with an optical microscope.
The oxidation experiments were carried out in the gold-image hot-stage of a Confocal Scanning Laser Microscope. During oxidation the sample surface was continuously scanned by using an imaging technique for obtaining high-resolution optical images [8]. The furnace chamber was evacuated and refilled with dry air, which was subsequently allowed to flow for 10 minutes. The flow rate was around 500 ml/s. The required heating time from RT to 800°C was 40s and the samples were maintained at this temperature for 15 minutes after which they were cooled to room temperature. Three samples of each chemistry listed in Table 1 were oxidized under the aforementioned conditions.

The samples were polished and marked with a Vickers Hardness Testing Machine. Marking were used to allow the recognition of specific places that could be of interest. Once the marks were made, the position of RE or Ti inclusions were easily locatable on the surface. Its evolution was followed with CLSM and the same places were examined again after oxidation. The marked surface was characterized before and after the experiments by a Philips XL Field Emission scanning electron microscope (SEM). The accelerating voltage determining the energy and wavelength of electrons in the electron beam was 10 kV. The resolution in the secondary electron mode at 10 kV was 3.5 nm at a working distance of 10 mm.

Cross sections were obtained by milling a rectangular hole (ca. 7 x 3 μm) on the surface with a Nova 600 DualBeam system. To avoid charge effects the surface was previously covered with 7.0 nm of Pt. The region of interest to be cross sectioned (around 20 μm) was encapsulated with 1 μm of Pt to avoid damage while milling. The surface was cross sectioned to a depth of 4-5 μm using a 30 kv Ga^+ ion beam with a current of ca. 0.5 nA. A serial cross-sectioning was carried out on sample labeled F_2. A cross-section was obtained first, and then by removing the material at the edge of this cross-section slice by slice at a thickness of 0.048 μm, sequential SEM images of cross-sections were taken after every slice was removed. In this way, a series of 100 images was obtained, from which the oxides layer was reconstructed in three-dimensional space using the software Amira 3.1.

Results

Surface oxide morphology

Optical images from etched surfaces of F_1, F_2 and F_3 are shown in Fig. 1. Large amounts of deformation (i.e. dislocations) left from prior cold work are observed and are concentrated at locations such as grain boundaries. There are fewer dislocations in F_2 and F_3 than in F_1. The grains are all elongated along the rolling direction and their size is of the order of a millimeter. The deformation in the samples and the morphology of the grains in F_1, F_2, F_3 indicate that the materials were not in a re-crystallized state. Particles were observed on the surface of all the samples which were rich in Ti for F_1 and Ce+La for F_2 and F_3. Since the RE (Ce+La) were added in the melt stage it is difficult to estimate the amount of RE that exists in soluble form vs. as oxide phases.

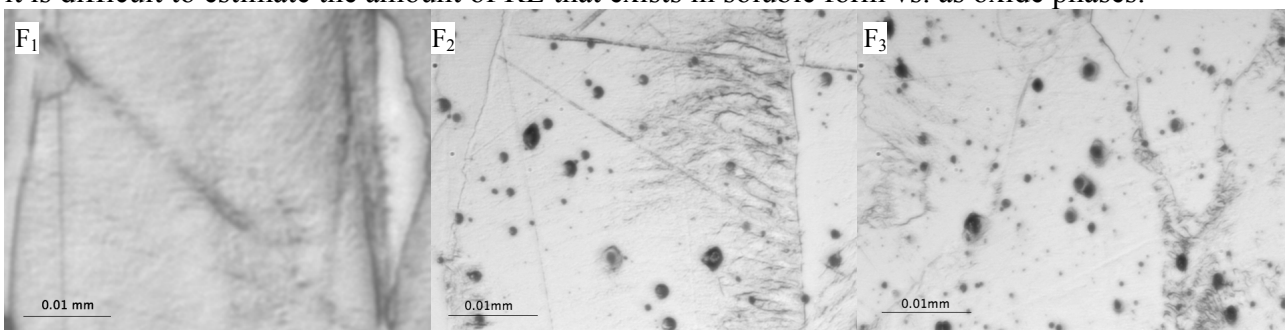

Figure 1. Optical images of the etched surface of F_1, F_2 and F_3.

In Fig. 2 SEM pictures for sample F_1 before and after 15 minutes oxidation are shown, as well as a CLSM image where ridges can be seen in the surface. Similar experiments were carried out for F_2 and F_3. Formation of ridges during oxidation was observed under CLSM in the three chemistries. However, in sample F_3, the ridges appeared to disappear with time and ridges were only clearly detectable in the SEM for post-experiment characterization in samples F_1 and F_2. In the case of F_3, only traces of what seemed to be ridges could be observed on the surface. During oxidation process no apparent difference was observed between regions near, at and far from Ti and RE-oxides. Post experiment characterization of the ridge can be seen in Fig. 3. The oxides that constitute the ridges are rich in Cr and Mn compared to the oxide nodules in the grain interiors.

SEM and EDS analysis of F_2 samples surface show an interesting phenomenon: oxide nodules containing RE surrounded by an area in which the chromium content is less than the average in the surface (33% *vs*. 40%) (Fig. 4A). A noticeable fraction of all the RE particles show this characteristic.

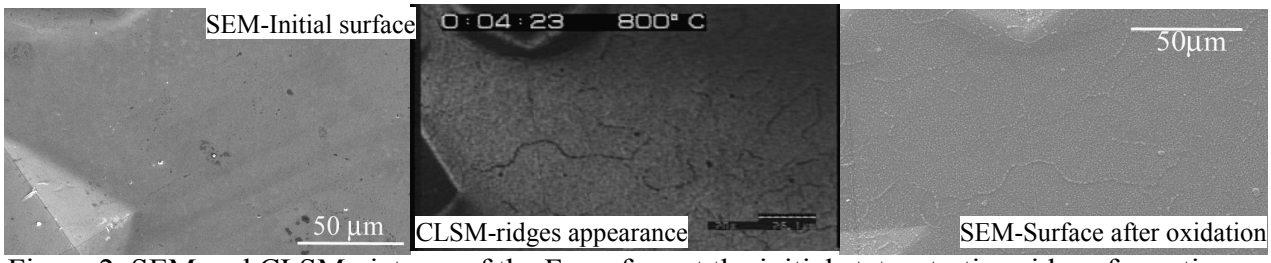

Figure 2. SEM and CLSM pictures of the F_1 surface at the initial state, starting ridges formation and after the oxidation.

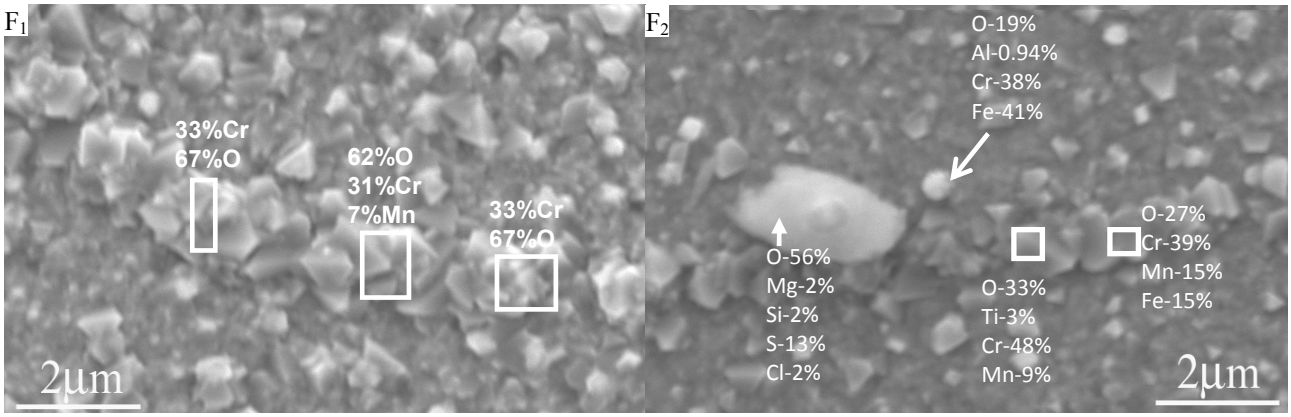

Figure 3. SEM pictures and EDS analysis of ridges formed on the surfaces of F_1 and F_2 after 15 minutes oxidation.

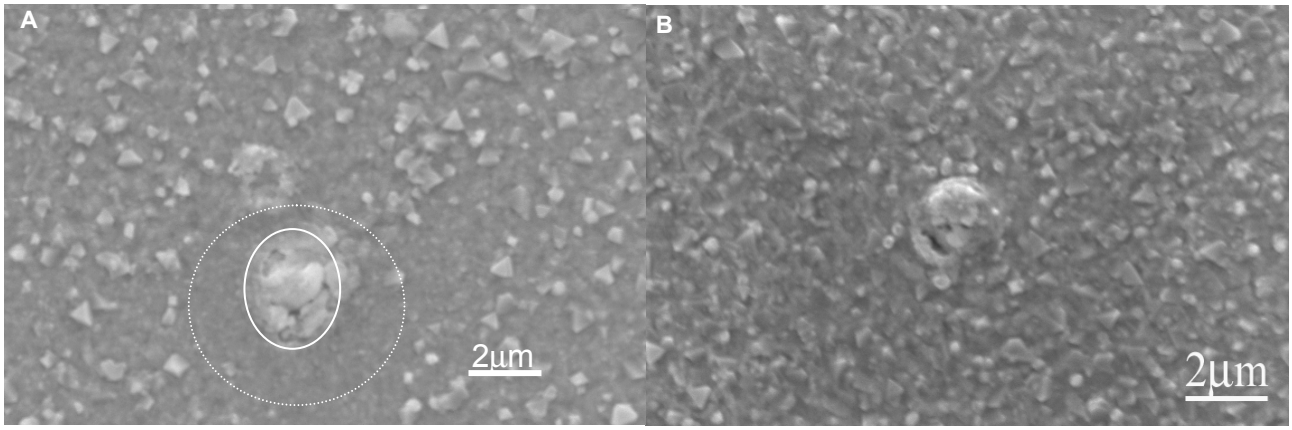

Figure 4. Characterization by SEM and EDS of particles formed during oxidation. A) Area surrounding RE particle (dotted line) distinct topographical features and a Cr content of 33 wt% lower than that of the average surface (~40 wt%); RE particle (solid line) with Ce 42.75 wt% and La 16.89 wt%. B) RE particle showing no clear surrounding Cr depleted zone.

Cross-sections

Figure 5 shows the cross sections of ridges in surfaces F_1, F_2 and F_3 obtained through FIB sectioning. In the cross-sections, ridges were visible in F_3 as well but it is less pronounced. It can be seen that ridges are in all three cases are located where the underlying metal grain boundaries intersect the surface/oxide-layer. The fact that the ridges are rich in Cr and Mn suggests that the metal grain boundaries act as preferential diffusion paths for these elements (Table 2). The oxide nodule size is also larger at the ridges compared to grain interiors, but this size diminishes with increasing RE content in the alloy.

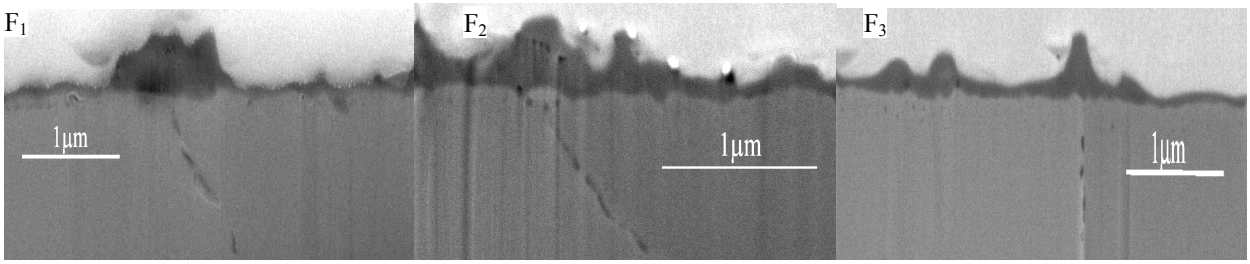

Figure 5. FIB cross sections showing scale ridges forming on top of alloy grain boundaries (F_1, F_2, F_3).

To strengthen the observed relationship between ridges and grain boundaries, a small area of oxide was reconstructed through serial cross-sectioning by FIB. The reconstructed oxide layer is shown in Fig. 6a. Ridges which formed a triple junction can be seen on the oxides layer (arrows pointed). Fig. 6b shows the reconstructed grain boundary planes. The white dotted lines indicated where the grain boundary planes intersected the oxides layer. Figures 6a and 6b show that the ridges on the oxides layer corresponded well to the grain boundary planes beneath.

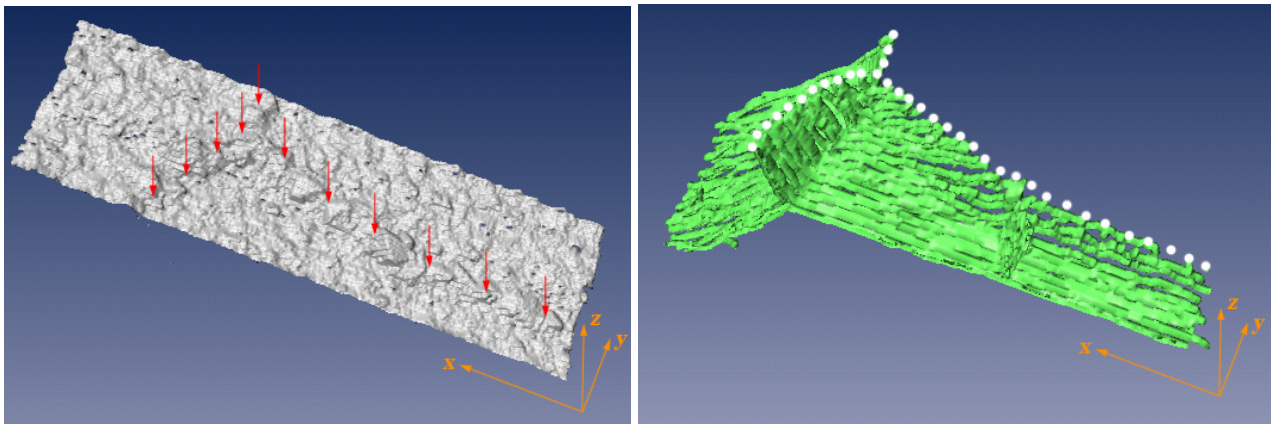

a) b)

Figure 6. Three dimensional reconstruction of a FIB serial cross sectioning of sample F_2.

Figure 7 A-C shows the cross-sections of the oxidized samples F_1, F_2 and F_3 that were obtained in the FIB across 2nd phase particles. The particles correspond to those found on the surface of the starting samples. The particles are rich in Ti in case of F_1 and RE (La and Ce) and Ti in cases of F_2 and F_3.

Surface EDS analysis found that chromium oxides formed preferentially over Ti particles (F_1), which are also rich in Mn (Fig. 7A). In the case of F_2 and F_3, chromium oxides would not only grow over the particles but also around them (Fig. 7B-C), suggesting that oxygen diffuses inwards along the particle/alloy interface. The oxide layer (excluding the particle) shown in Fig. 7 is around 0.14 micron.

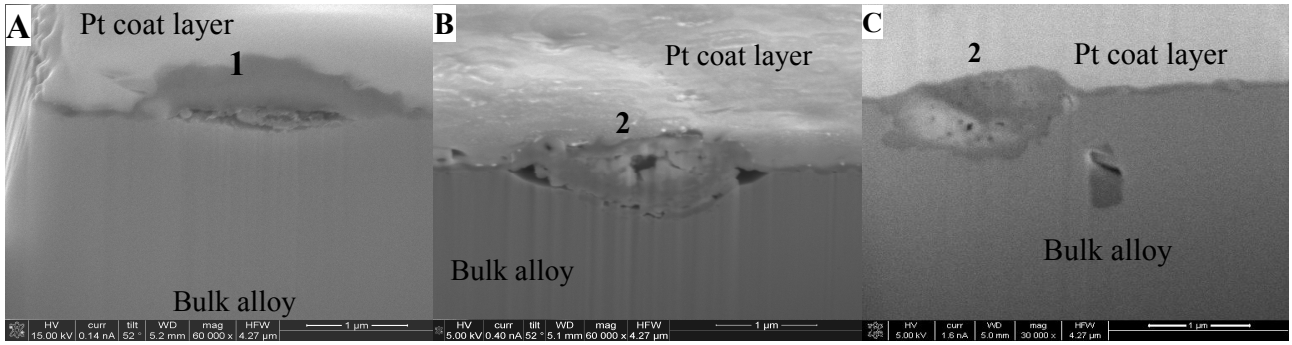

Figure 7. **A**) F_1 FIB cross section, **B**) F_2 FIB cross section**,** **C**) F_3 FIB cross section. **1**: big particles formed in F_1 over Ti-oxides. **2**: RE nucleation sites. Cr and Mn oxides grow in these sites.

Discussion

While sample F_1 does not contain rare-earth elements, it does contain Ti. The Ti-ion is not large but Ti is comparably reactive [2] and therefore regions that included Ti were studied. Ionic radii for elements which influence scale growth are: Cr^{+3} 0.6 Å < Mg^{+2} 0.65 Å < Ti^{+4} 0.68 Å < Y^{+3} 0.93 Å < Ce^{+4} 1.01 Å < La^{+3} 1.87 Å.

RE oxides inclusions acting as nucleation sites for chromium oxides have been reported in several publications [2, 3, 5]. These experiments show such RE-inclusion particles being buried by the evolving scale during the oxidation process (Figs. 4 and 7) but there is no indication that the scale grain structure is refined at those locations.

The RE after oxidation can be observed both as having been buried (as in F_2) and as protuberances over the surface. In this case it was not detected a clear depletion area around RE particles as in F_2 (Fig. 4).

Pure chromium oxide nodules are more abundant in F_1 (Fig. 3). Higher surface coverage by these particles is observed in the sample without RE. SEM post-analysis of the three surfaces confirm that the higher the RE content, the less chromium oxide particles over the surface. When RE are present the scale that forms is mainly iron and chromium oxides (spinel), meaning that from F_1 to F_3 spinel areas become larger and a decrease in ridge abundance and size was observed (Fig. 5).

According to the obtained results, what could be occurring in the presence of RE addition is represented in Fig. 8. The high temperature oxidation process implies migration of Cr (mainly) and other elements as Mn diffusion through the bulk towards the surface. The diffusion of Mn and Cr through grain boundaries was shown to be preferential (Fig. 5). The presence of RE-oxides would influence the process in two ways: acting as nucleation sites for chromium oxides (Fig. 7) and blocking Cr and Mn diffusion through grain boundaries. The decreasing size in the ridges with RE presence (Fig. 5) has been found so far for this hypothesis.

The composition of the oxide particles and ridges after oxidation is seen in Table 2 where it can be seen that the ridges are richer in Mn and leaner in Fe when compared to the regions away from the ridges. The fact that the location of ridges coincide with the underlying metal grain-boundaries suggests that the scale growth is not completely controlled by ion-diffusion at this stage of the transient scale evolution and that fast-path diffusion through the metal-grain boundaries contribute to a faster scale growth. The starting surface grain size does not correspond to the separation distance between ridges but this is not surprising since the samples most likely underwent re-crystallization during heating due to the high amount of dislocations (Fig. 1).

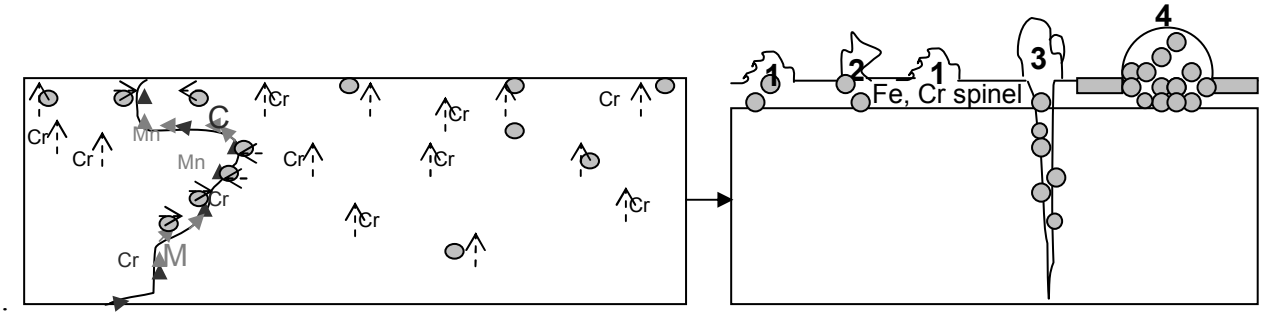

Figure 8. Schematic representing the mechanism of what is possibly happening during the oxidation in presence of RE. **1** and **2:** particles formed on the surface (rich mainly in chromium oxides). Some of them contain Mn oxides. **3**: ridges of Cr and Mn oxides formed on the alloy grain boundaries. **4**: Potential RE nucleation sites. Cr and Mn oxides grow in these sites. ▭ - Spinel areas with less content in Cr. ○ - RE particles.

Morphological and compositional analysis of oxidized surfaces.

Alloy	final surface grain size [μm^2]	separation distance between ridges [μm]	nodule size at ridge [μm]	nodule size away from ridge [μm]	average composition of scale at ridge [wt%]	average composition of scale nodules away from ridge [wt%]
F_1	69.7	65	~1	~0.6	O ~35, Cr ~55, Mn ~9	O ~35,Cr ~54, Mn ~8, Fe ~0.5, Al~2
F_2	160.6	82	~0.7	~0.7	O ~33, Cr ~53, Mn ~11, Ti ~2	O ~56, Cr ~40, Mn ~4
F_3	63.5	Ridges not observable	Ridges not observable	~1.1	Ridges not observable	O ~22, Cr ~37, Mn ~16, Fe ~22, Al ~0.3

Table 2. Structural features of the surfaces F_1, F_2 and F_3 after 15 minutes oxidation.

Conclusions

Scale evolution in Fe-22 wt.% Cr alloys at 800 ^{o}C in dry air after 15 minutes oxidation was compared in samples containing (i) no rare earth (RE), (ii) 120 ppm of La + 270 ppm of Ce and (iii) 290 ppm La + 610 ppm Ce.

Cr and Mn oxides grow preferentially on Ti and RE particles. Cr-oxide also forms underneath the particles and this suggests that oxygen transport takes place into the alloy.

A noticeable fraction of the RE particles in F_2 alloy showed a region around them that was depleted in Cr.

The samples showed oxide ridges forming at locations where metal-grain boundaries intersected the surface, suggesting that the metal grain boundaries act as preferential diffusion paths for Cr and Mn.

The size of the ridges decreased with increasing RE addition, suggesting that the latter could be blocking the fast-path diffusion.

Acknowledgments

This work was carried out under the contract DE-AC26-04NT41817.

References

[1] J. Stringer, B. A. Wilcox and R. I. Jaffee: Oxid. Met. Vol. 11 (1972), p. 5.

[2] G. M. Ecer and G. H. Meier: Oxid. Met. Vol. 13 (1979), p. 159.

[3] M. Ecer, Singh and G. H. Meier: Oxid. Met. Vol. 18 (1982), p. 55.

[4] C. S. Giggins and F. S. Pettit: Met. Trans. Vol. 2 (1971), p. 1071.

[5] G. M. Ecer and G. H. Meier: Oxid. Met. Vol. 13 (1979), p. 119.

[6] R. Thanneeru, S. Pati., S. Deshpande and S. Seal: Act. Mat. Vol. 55 (2007), p. 3457.

[7] M. Hajduga and J. Kučera: Oxid. Met. Vol. 29 (1988), p. 121.

[8] H. Yin, H. Shibata, T. Emi and M. Suzuki: ISIJ Int. Vol. 37 (1997), p. 936.

Diffusion in Solids and Liquids IV
doi:10.4028/3-908454-50-6

Fundamental Studies on the Transient Stages of Scale Growth in Fe-22 wt.% Cr Alloys

doi:10.4028/3-908454-50-6.425